

# Ground state and finite temperature behavior of $\frac{1}{4}$ -filled band zigzag ladders

R. Torsten Clay<sup>1,2\*</sup>, Jeong-Pil Song<sup>1</sup>, Saurabh Dayal<sup>1</sup>, and Sumit Mazumdar<sup>3</sup>

<sup>1</sup>Department of Physics and Astronomy and HPC<sup>2</sup> Center for Computational Sciences, Mississippi State University, Mississippi State, MS, 39762

<sup>2</sup>Institute for Solid State Physics, The University of Tokyo, Kashiwa 277-8581, Japan

<sup>3</sup>Department of Physics, University of Arizona, Tucson, AZ, 85721

We consider the simplest example of lattice frustration in the  $\frac{1}{4}$ -filled band, a one-dimensional chain with next-nearest neighbor interactions. For this zigzag ladder with electron-electron as well as electron-phonon interactions we present numerical results for ground state as well as thermodynamic properties. In this system the ground state bond distortion pattern is independent of electron-electron interaction strength. The spin gap from the ground state of the zigzag ladder increases with the degree of frustration. Unlike in one-dimension, where the spin-gap and charge ordering transitions can be distinct, we show that in the ladder they occur simultaneously. We discuss spin gap and charge ordering transitions in  $\frac{1}{4}$ -filled materials with one, two, or three dimensional crystal structures. We show empirically that regardless of dimensionality the occurrence of simultaneous or distinct charge and magnetic transitions can be correlated with the ground state bond distortion pattern.

KEYWORDS: ladder, spin gap, lattice frustration, 1/4 filling, organic conductors

## 1. Introduction

The consequences of geometric lattice frustration on ground and excited state behavior of spin systems have been widely studied over the past two decades.<sup>1,2</sup> Even as many of the issues are still being debated for the complex two- and three-dimensional (2D and 3D) lattices, consensus on some of the simpler models have been reached. One such model frustrated system is the spin- $\frac{1}{2}$  zigzag ladder, with nonzero antiferromagnetic exchanges  $J_1$  and  $J_2$  between nearest and next-nearest neighbor spins. The ground state here is a valence bond solid (VBS) for  $J_2 = 0.5J_1$ ,<sup>3,4</sup> and is dimerized for  $J_2 \geq 0.2411J_1$ ,<sup>5,6</sup> where the excitations are spin solitons.<sup>7,8</sup> Some theoretical results exist also for  $J_2 > J_1$ .<sup>9-11</sup>

Spin Hamiltonians are restricted to a charge per site  $\rho = 1$  ( $\frac{1}{2}$ -filled band) and are obtained in the limit of very large on-site Hubbard repulsion  $U$  between electrons or holes where there are no charge degrees of freedom. The literature on frustrated non- $\frac{1}{2}$ -filled bands, where the charge degrees of freedom are non-vanishing even for  $U \rightarrow \infty$ , remains relatively sparse. Much of the literature on non- $\frac{1}{2}$ -filled band frustrated systems is for  $\rho = \frac{1}{2}$ , or the  $\frac{1}{4}$ -filled band, which is of interest both because under certain conditions it can be described within an effective  $\frac{1}{2}$ -filled band picture,<sup>12-14</sup> and because there exist many  $\frac{1}{4}$ -filled band frustrated materials, both organic and inorganic, that exhibit novel behavior including charge, spin and orbital-ordering, and superconductivity (see below). We have recently shown that there is a strong tendency to form local spin-singlets in the  $\frac{1}{4}$ -filled band with strong electron-electron interactions, in both one dimension (1D) and 2D, and especially in the presence of lattice frustration, which enhances quantum effects.<sup>15,16</sup> The frustration-driven singlet formation does not occur if only the frustrating Coulomb interactions are included;<sup>17</sup> the inclusion of the frustrating electron-hopping integral, with or without the corresponding Coulomb interactions is essential. Singlet formation in the  $\frac{1}{4}$ -filled band is accompanied by charge-ordering

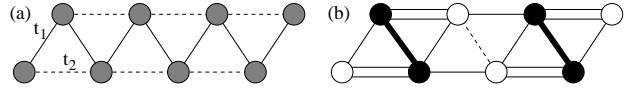


**Fig. 1.** Zigzag ladder lattice and ground state configurations for density  $\rho = \frac{1}{2}$ . (a) The ground state for  $t_2/t_1 > 1.707$  has uniform charges and bonds. (b) For  $t_2/t_1 < 1.707$ , the ground state is a PEC with coexisting charge and bond order. Filled (open) circles correspond to sites with large (small) charge density. The heavy line indicates the strongest (spin-singlet) bond. Double, single, and dotted lines indicate strong, intermediate, and weak bonds, respectively.

(CO), leading to what we have termed as a *paired-electron crystal* (PEC), which consists of pairs of singly-occupied sites separated by pairs of vacant sites. The PEC is the  $\frac{1}{4}$ -filled band equivalent of the VBS. The difference from the standard VBS lies in the possibility that the PEC gives way to a *paired-electron liquid* under appropriate conditions, which might then lead to superconductivity. Clearly it is desirable to extend our current work on the ground state of the PEC to excited states.

In the present paper, we discuss theoretical results for the PEC that occurs in the simplest  $\frac{1}{4}$ -filled frustrated lattice with interacting electrons. The lattice geometry here is the same as in the spin zigzag ladder (see Fig. 1(a)), with nearest and next nearest neighbor electron hopping matrix elements  $t_1$  and  $t_2$ , respectively. In our previous work on the ground state of the  $\frac{1}{4}$ -filled band zigzag ladder,<sup>18</sup> we had shown that in the presence of electron-lattice coupling (either nearest neighbor along the zigzag direction, or second neighbor, or both), and for  $t_2/t_1$  less than a critical value  $(t_2/t_1)_c$  (see below) there occurs a coupled bond-charge density wave (BCDW), as shown in Fig. 1(b). Alternate rungs of the zigzag ladder are occupied by singlet spin-coupled charge-rich sites, and charge-poor sites occupy the other set of rungs. The CO pattern here characterizes the BCDW as a PEC. We discuss below the nature of the ground state in this system for the complete parameter range  $t_2/t_1 < (t_2/t_1)_c$ . We also present numerical results

for spin excitations and thermodynamics for the  $\frac{1}{4}$ -filled band zigzag ladder within the interacting electron Hamiltonian and discuss applications of the model to real systems.

Although our actual work is limited to the zigzag ladder, our analysis leads to an empirical understanding of a perplexing observation in the  $\frac{1}{4}$ -filled band systems with interacting electrons in general. In many such systems, irrespective of dimensionality, there often are two transitions, (i) a high temperature metal-insulator (MI) transition at  $T_{\text{MI}}$  that is accompanied by CO without any perceptible effect on the magnetic behavior, and (ii) a second insulator-insulator transition at a lower temperature  $T_{\text{SG}}$  where a spin gap (SG), seen in the magnetic susceptibility, occurs. In a second class of systems with nearly identical chemical constituents there occurs however a single transition with  $T_{\text{MI}} = T_{\text{SG}}$ . We point out a well-defined correlation between this “two-versus-one” transition and the pattern of the bond distortion in the spin-gapped phase. Furthermore, many interacting  $\frac{1}{4}$ -filled band materials are superconducting, often under pressure. There appears to exist a correlation also between superconductivity and the bond distortion pattern at the lowest temperatures.

The organization of the paper is as follows. In Section 2 we introduce our Hamiltonian for the  $\frac{1}{4}$ -filled band zigzag ladder. In Section 3 we present a brief summary of the earlier results for the 1D limit of this model,<sup>19–23</sup> and for the ground state of the zigzag ladder.<sup>18</sup> Two different bond distortion patterns, accompanied however with the same charge distortion pattern are possible in the 1D limit. We point out the two bond distortion patterns correspond to two different mappings of the  $\frac{1}{4}$ -filled band to effective  $\frac{1}{2}$ -filled bands. In the 1D limit both mappings are valid. In contrast, only one mapping is applicable to the zigzag ladder, and there is a single unambiguous PEC here. The results of our numerical calculations for the zigzag ladder are presented in Section 4, where we discuss both ground state and temperature-dependent behavior. In Section 5 we discuss the implications of our results for real  $\frac{1}{4}$ -filled materials. Appendix A contains details of the numerical method, based on a matrix-product state (MPS) representation, used for our large-lattice calculations. Appendix B contains details of the finite-size scaling of our ground-state calculations.

## 2. Theoretical model and parameter space

The Hamiltonian for the zigzag ladder is

$$\begin{aligned}
 H = & -t_1 \sum_i (1 + \alpha_1 \Delta_{i,i+1}) B_{i,i+1} + \frac{1}{2} K_1 \sum_i \Delta_{i,i+1}^2 \\
 & - t_2 \sum_i (1 + \alpha_2 \Delta_{i,i+2}) B_{i,i+2} + \frac{1}{2} K_2 \sum_i \Delta_{i,i+2}^2 \\
 & + \sum_i (U n_{i\uparrow} n_{i\downarrow} + V_1 n_i n_{i+1} + V_2 n_i n_{i+2}). \quad (1)
 \end{aligned}$$

In Eq. 1  $B_{i,j} = \sum_{\sigma} (c_{j,\sigma}^{\dagger} c_{i,\sigma} + H.c.)$  is the kinetic energy operator for the bond between sites  $i$  and  $j$ , where  $c_{i,\sigma}^{\dagger}$  creates an electron of spin  $\sigma$  on site  $i$ .  $n_{i\sigma} = c_{i,\sigma}^{\dagger} c_{i,\sigma}$  is the density operator, and  $n_i = n_{i\uparrow} + n_{i\downarrow}$ .  $t_1$  and  $t_2$  are hopping integrals along the zigzag rung direction and the rail direction, respectively, as shown in Fig. 1. The lattice may also be viewed as a 1D chain with nearest neighbor hopping  $t_1$  and frustrating

below, however, we will imply  $t_2 = 0$  and  $V_2 = 0$ . We give energies in units of  $t_1$  and fix  $t_1=1$ .  $\Delta_{i,j}$  is the deformation of the bond between sites  $i$  and  $j$ ;  $\alpha_1$  and  $\alpha_2$  are the inter-site electron-phonon (e-p) coupling constants with corresponding spring constants  $K_1$  and  $K_2$ , which for simplicity we choose to be identical in the  $t_1$  and  $t_2$  directions ( $\alpha_1 = \alpha_2 \equiv \alpha$  and  $K_1 = K_2 \equiv K$ ). For all results below we fix  $K_1 = K_2 = 2$ . We have omitted intra-site e-p coupling terms in Eq. 1, as apart from changing the strength of the charge order, they do not greatly change the thermodynamic properties.<sup>22</sup>  $U$  is the onsite Coulomb interaction and  $V_1$  and  $V_2$  are the nearest-neighbor Coulomb interactions for  $t_1$  and  $t_2$  bonds. We will consider only the case  $V_1 = V_2 = V$ . In the 1D limit, the ground state is a Wigner crystal (WC) for  $V_1 > V_1^c$ , where  $V_1^c = 2|t_1|$  for  $U \rightarrow \infty$  and is larger for finite  $U$ . Our discussions of the 1D limit are for  $V_1 < V_1^c$ . All calculations use periodic boundary conditions.

## 3. Summary of earlier results.

Given the complexity of our results, it is useful to have a brief summary of our earlier results. While the numerical results for the 1D limit and the ground state of the zigzag ladder have been presented before, the mappings of the ground states to the effective  $\frac{1}{2}$ -filled band model that we discuss below give new insight.

### 3.1 1D limit

For moderate to strong electron-electron (e-e) interactions but  $V_1 < V_1^c$ , the  $\frac{1}{4}$ -filled band is bond- or charge-dimerized at  $T < T_{\text{MI}}$ . In either case the ground state enters a spin-Peierls (SP) phase<sup>22,23</sup> for  $T < T_{\text{SG}}$ . We show in Fig. 2(a) a schematic of the bond-dimerized phase, with site charge densities 0.5, strong intradimer bonds and weak interdimer bonds. The dimer unit cells (the boxes in the figure) containing a single electron can be thought of as effective sites, which leads to the effective  $\frac{1}{2}$ -filled band description in this case.<sup>14</sup> The description of the SP state is then as shown in Fig. 2(b), with alternating *inter*-dimer bonds. The overall pattern of bond strength here is  $\cdots$  Strong-Weak-Strong-Weak'  $\cdots$  (SWSW'),<sup>19,21,24</sup> Unlike the true  $\frac{1}{2}$ -filled band, however, the charge degrees of freedom internal to the dimer unit cell are relevant in the  $\frac{1}{4}$ -filled band, and the charge distribution is as shown in the Fig. 2(b). The coexisting charge order pattern is written as  $\cdots 1100 \cdots$ , where ‘1’ (‘0’) denotes site charge density of  $0.5 + \delta$  ( $0.5 - \delta$ ). The CO amplitude  $\delta$  varies with e-e and e-p interaction strengths. Nearest-neighbor spin-singlet coupling between the electrons on charge-rich ‘1’ sites that are linked by the W' inter-dimer bond gives the spin gap of this SP phase. This coexisting broken symmetry state has been termed a BCDW,<sup>19,21,24</sup> and is the simplest example of the PEC found more generally in  $\frac{1}{4}$ -filled systems beyond the 1D limit.<sup>15,16</sup> Finite temperature phase transition to the SWSW' phase, starting from the uniform phase and through the dimer phase of Fig. 2(a), has been demonstrated within an extended Hubbard model that incorporated interchain interactions at a mean-field level.<sup>25</sup>

The pattern of bond order modulation in the 1D PEC is not unique but depends on the strength of e-e interactions.<sup>19</sup> The bond-order pattern that dominates for relatively weaker e-e interactions, or for relatively strong e-p interaction has the

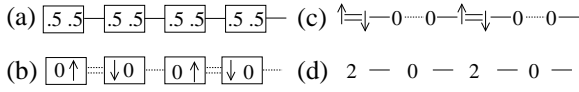


**Fig. 2.** (a) Bond-dimerized phase with uniform charge density. Boxes denote dimer units. (b) SP state evolving from (a), with bond pattern SWSW'. Strong 'S' dimer bonds are represented by boxes enclosing two sites. Zeroes indicate sites with charge density  $0.5 - \delta$  while spins indicate sites with charge density  $0.5 + \delta$ . Double dotted bonds are stronger than single-dotted bonds, but weaker than the dimer bonds. (c) Bond pattern SMWM found in the case of relatively weaker e-e interactions. Here double lines indicate the strongest 'S' bonds, single lines medium strength 'M' bonds, and dotted lines weak 'W' bonds. (d) Effective  $\frac{1}{2}$ -filled band model for (c).

portantly, in this bond pattern the coexisting charge modulation pattern is again  $\cdots 1100 \cdots$  but the spin singlets now coincide with the strongest 'S' *intra*-dimer bonds (Fig. 2(c)). As shown in Fig. 2(d), the corresponding effective  $\frac{1}{2}$ -filled band is now different; pairs of sites with large (small) charge densities are now mapped onto effective sites with charge density 2 (0). The bonds between the effective sites are now equivalent, and the effective state is now a  $\frac{1}{2}$ -filled band *site*-diagonal CDW, which is known to have a single transition where charge and magnetic gaps open simultaneously. Further, as the strongest bond coincides with the location of the spin-singlet, this state is also expected to have a larger SG and transition temperature than  $T_{SG}$  in the SWSW' case. A simple physical picture for two-versus-one transition is thus obtained from the 1D study: if the strongest bonds are between a charge-rich and a charge-poor site, the spin-singlet formed are inter-dimer and there will occur two transitions; if, however, the strongest bond is a 1-1 bond, the spin singlet is located on an *intra*-dimer bond and there is a single transition.

### 3.2 Zigzag ladder

The energy dispersion relation in the zigzag ladder in the noninteracting limit is a sum of two terms,

$$E(k) = -2t_1 \cos(q) - 2t_2 \cos(2q). \quad (2)$$

Here  $q$  refers to a wavenumber along the  $t_1$  direction, viewing the ladder as a 1D chain with second-neighbor interactions. The topology of the bandstructure changes at  $t_2/t_1 = (t_2/t_1)_c = (2 + \sqrt{2})/2 = 1.707 \cdots$ ; for  $t_2/t_1 < (t_2/t_1)_c$  the Fermi surface consists of two points at  $q = k_F = \frac{\pi}{4}$ , while for  $t_2/t_1 > (t_2/t_1)_c$  there are four such points. In the presence of e-p coupling the ground state is then unstable<sup>18</sup> to a Peierls distorted state for  $t_2/t_1 < (t_2/t_1)_c$ . As in 1D, the ground state in the distorted region again has  $\cdots 1100 \cdots$  CO and a spin gap.

Importantly, for the  $\rho = \frac{1}{2}$  zigzag ladder, there is no WC state with a charge order *distinct* from the  $\cdots 1100 \cdots$  charge order found in the PEC (for  $V_1 \sim V_2$ ). In the zigzag ladder, the WC charge pattern  $\cdots 1010 \cdots$  CO can be placed along the two  $t_2$  directions in two different ways, both of which lead to the same PEC state shown in Fig. 1(b). Placing the WC CO pattern  $\cdots 1010 \cdots$  along the zigzag direction would place all charge on a single  $t_2$  chain and is stable only in the limit  $V_1 \gg V_2$ . Thus only the PEC of Fig. 1(b) is stable for realistic  $V_1 \sim V_2$ . As we show below, this has important consequences for both the number of transitions expected in the zigzag ladder and the nature of the spinon excitations.

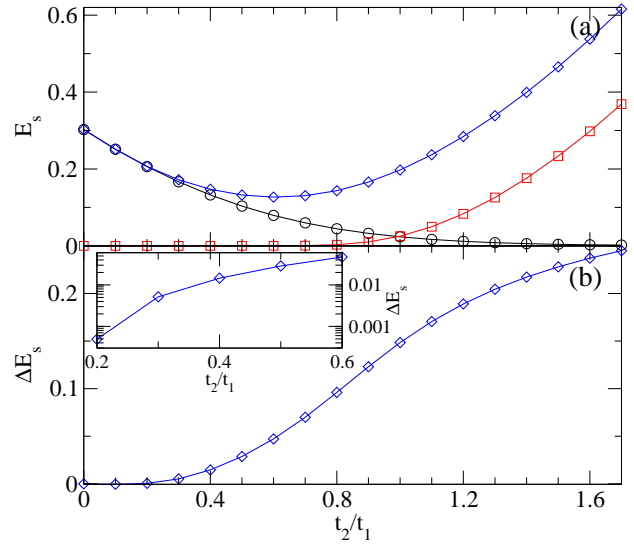


**Fig. 3.** (color online) (a)  $E_s$ , the per site spring constant energy term in Eq. 1, as a function of  $t_2/t_1$  for a 256 site ladder with  $U = V = 0$ . Electron-phonon parameters are  $\alpha_1 = 1.6, \alpha_2 = 0$  (circles);  $\alpha_1 = 0, \alpha_2 = 1.6$  (squares); and  $\alpha_1 = 1.6, \alpha_2 = 1.6$  (diamonds). (b) Cooperative enhancement  $\Delta E_s$  as a function of  $t_2/t_1$  (see text). The inset shows the small  $t_2/t_1$  region in more detail.

## 4. Numerical Results for the zigzag ladder

We use two different numerical methods to solve Eq. 1. For the ground state order parameters and the spin gaps in the interacting case we use a new variational quantum Monte Carlo (QMC) method using a MPS basis.<sup>26</sup> For quasi-1D systems, this MPS-QMC method provides accuracy similar to that of the Density Matrix Renormalization Group (DMRG)<sup>27,28</sup> method. Similar methods using MPS representations have predominantly been used to study quantum spin systems. Our results here show however that they may be successfully applied to electronic models as well. Details on the application of this method to Hubbard-type models are discussed in Appendix A. For finite temperatures our calculations are for zero e-p interactions ( $\alpha_1 = \alpha_2 = 0$ ). This is because information about the tendency to distortion exists in the wavefunction even without inclusion of explicit e-p interactions.<sup>29</sup> We use here the standard determinantal QMC method.<sup>30</sup> While the lowest temperatures achievable by this method are limited by the Fermion sign problem, in the present system for density  $\rho = \frac{1}{2}$ , inverse temperatures of  $\beta \approx 10 - 16$  are reachable for parameters  $U \approx 4$  and  $V = 0$ .

### 4.1 Charge order, bond periodicity, and spin gap

We first consider the solution of Eq. 1 in the limit of zero e-e interactions ( $U = V = 0$ ). Because Eq. 1 includes e-p coupling in both the  $t_1$  and  $t_2$  directions, the variation of the lattice distortion amplitude with the ratio  $t_2/t_1$  is nontrivial. The total spring constant energy  $E_s$ , the sum of  $K_1$  and  $K_2$  terms in Eq. 1, is a convenient measure of the strength of the lattice distortion. Fig. 3(a) shows  $E_s$  as a function of  $t_2/t_1$  for a 256 site ladder. Three different choices for e-p couplings are shown: (i)  $\alpha_1 = \alpha, \alpha_2 = 0$ ; (ii)  $\alpha_1 = 0, \alpha_2 = \alpha$ ; and (iii)  $\alpha_1 = \alpha_2 = \alpha$ . In the first case with e-p coupling only along the zigzag direction, the lattice distortion is strongest when  $t_2 = 0$ , and vanishes continuously at  $(t_2/t_1)_c$ . In the second

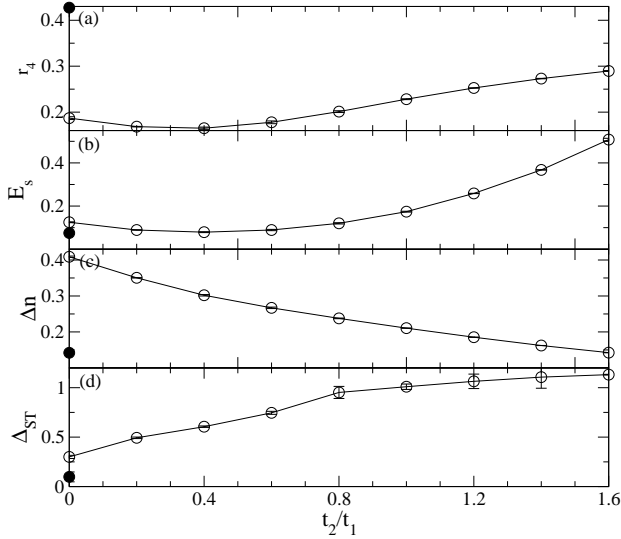


**Fig. 4.** Order parameters versus  $t_2/t_1$  for the zigzag ladder with  $U = 6$ ,  $V = 1$ , and  $\alpha = 1.6$ . Results are finite-size scaled from 20, 28, 36, and 60 site lattices. (a)  $4k_F$  component of the lattice distortion, and (b) spring energy per site,  $E_s$ , (c) charge disproportionation  $\Delta n$ , and (d) singlet-triplet gap  $\Delta_{ST}$ . Open symbols are for  $V = V_1 = V_2$ , and filled symbols at  $t_2/t_1 = 0$  are for  $V = V_1, V_2 = 0$  (see text).

case with e-p coupling only along the  $t_2$  bonds, the strength of the distortion increases with  $t_2$ . Putting these two effects together, the strength of the lattice distortion in the general case with  $\alpha_1$  and  $\alpha_2$  nonzero shows a minimum at an intermediate value of  $t_2/t_1$ , as seen in Fig. 3. The precise  $t_2/t_1$  value of this minimum will depend on the specific choices for  $\alpha_1$  and  $\alpha_2$ .

Fig. 3(a) also shows that the  $t_2$  and  $t_1$  lattice distortions act *cooperatively*—the total lattice distortion for both  $\alpha_1$  and  $\alpha_2$  nonzero is considerably stronger than the sum of the independent distortions. In Fig. 3(b), we plot a quantitative measure of the cooperative enhancement,  $\Delta E_s = E_s(\alpha_1 = \alpha_2 = \alpha) - (E_s(\alpha_1 = \alpha, \alpha_2 = 0) + E_s(\alpha_1 = 0, \alpha_2 = \alpha))$ , as a function of  $t_2/t_1$ .  $\Delta E_s$  increases continuously with  $t_2/t_1$ , and as shown in the inset is nonzero even for small values of  $t_2/t_1$ . As we will discuss further in Section 5, this cooperative effect also has potentially important consequences for materials—if both  $\alpha_1$  and  $\alpha_2$  are nonzero, near  $(t_2/t_1)_c$  the lattice distortion changes abruptly.

A key difference between the  $\rho = \frac{1}{2}$  zigzag ladder and the single chain is that in the ladder the bond pattern of the PEC remains SMWM regardless of the strength of e-e interactions. In 1D the displacement of site  $j$  from equilibrium,  $u_j$  ( $\Delta_{j,j+1} = u_{j+1} - u_j$  in Eq. 1), can be written as<sup>19</sup>

$$u_j = u_0[r_2 \cos(2k_F j - \theta_2) + r_4 \cos(4k_F j - \theta_4)], \quad (3)$$

where  $r_2$  and  $r_4$  are relative components of the period-4  $2k_F$  and period-2  $4k_F$  lattice distortions and  $u_0$  is an overall amplitude.  $r_2$  and  $r_4$  are normalized such that  $r_2 + r_4 = 1$ . The SMWM bond pattern corresponds to  $r_4 < 0.41$  while the SWSW' pattern<sup>19</sup> has  $r_4 > 0.41$ . In both cases  $\theta_2 = \frac{\pi}{4}$  and  $\theta_4 = 0$ . Note that  $\Delta_{j,j+2}$  in Eq. 1 is an independent lattice distortion of the  $t_2$  bonds and has no counterpart in the 1D model.

While the PEC occurs in the thermodynamic limit for  $t_2/t_1 < (t_2/t_1)_c$  and  $\alpha = 0^+$ , in finite lattices a finite e-p coupling is required to observe the broken-symmetry ground state. We have chosen the e-p coupling strengths  $\alpha$  and  $g$  just

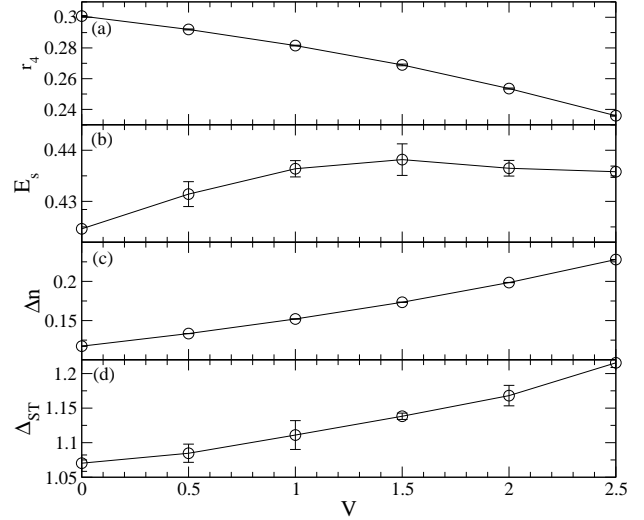


**Fig. 5.** Dependence of order parameters on  $V$ . Results are finite-size scaled from 20, 28, 36, and 60 site lattices. Quantities plotted in panels (a)-(d) are as defined in Fig. 4. Here  $t_2/t_1 = 1.5$ ,  $U = 6$ , and  $\alpha = 1.6$ .

larger than the minimum required for the ground and triplet states to be Peierls distorted. The strength of the lattice distortion depends on the values of  $\alpha$  and  $\beta$  and therefore results here should not be directly compared to experimental values.

In Fig. 4 we plot the finite-size scaled values of several order parameters determined self-consistently versus  $t_2/t_1$  for  $\alpha = 1.6$ ,  $U = 6$ , and  $V = 1$ . Exact and MPS-QMC calculations were performed for 20, 28, 36, and 60 site lattices. Details of the finite-size extrapolation are given in Appendix B.

Fig. 4(a) shows the  $4k_F$  lattice distortion strength and Fig. 4(b) the spring constant energy per site (including both  $t_1$  and  $t_2$  lattice distortions). Fig. 4(c) shows the charge disproportionation  $\Delta n$ , defined as the difference between the charge density on charge-rich and charge-poor sites. The singlet-triplet gap defined as  $\Delta_{ST} = E(S = 1) - E(S = 0)$  is plotted in Fig. 4(d). Note that two different ‘1D’ limits are shown in Fig. 4 at  $t_2/t_1 = 0$ : either including the second neighbor Coulomb interaction ( $V_2 = V$ , open symbols), or with only nearest-neighbor Coulomb interactions ( $V_2 = 0$ , filled symbols).

Focusing first on the  $t_2/t_1 = 0$  limit, the bond pattern is SMWM in the case where  $V_2$  is nonzero, as is found in the 1D weakly correlated band.<sup>19</sup> In the more traditional 1D with no second-neighbor  $V_2$ , the bond distortion pattern is SWSW' for  $U = 6$ ,  $V = 1$  with  $r_4 > 0.41$  (filled circle). For equal e-p coupling, the lattice distortion energy,  $\Delta n$ , and  $\Delta_{ST}$  are all stronger when the bond pattern is SMWM. Away from the 1D limit,  $r_4$  increases with increasing  $t_2/t_1$  but is always less than the 0.41 that would be necessary to reach the SWSW' bond pattern. The amplitude of the lattice distortion measured by the spring constant energy in Fig. 4(b) shows a minima at intermediate  $t_2/t_1$  as in the non-interacting case. Surprisingly,  $\Delta n$  *decreases* as the lattice distortion becomes stronger—this is one significant difference from the 1D chain BCDW state where  $\Delta n$  follows the strength of the bond distortion. Reference<sup>18</sup> showed that the spin gap in the PEC state of the zigzag ladder is larger than the gap in the single chain having the same  $\Delta n$ . As Fig. 4(d) shows, the gap in the ladder increases

with  $t_2/t_1$ , and is largest near  $(t_2/t_1)_c$ .

The  $U$  interaction weakens the PEC in the zigzag ladder (not shown). This decrease is, however, weaker than in the 1D chain.<sup>18</sup> In Fig. 5 we show the results of varying  $V$  while keeping other parameters ( $t_2/t_1 = 1.5$ ,  $U = 6$ , and  $\alpha = 1.6$ ) fixed. Even at large  $V$  ( $V > U/2$ ), as expected we did not find any transition to a distinct WC state; in all cases the CO pattern is  $\cdots 1100 \cdots$  along the zigzag direction. Contrary to what occurs in the 1D limit, the  $4k_F$  component of the bond distortion actually *decreases* with increasing  $V$ . While in 1D  $V$  destabilizes the  $\cdots 1100 \cdots$  CO, in the zigzag ladder, this effect in the ladder along the  $t_1$  direction is countered by  $V_2$ , which prefers  $\cdots 1010 \cdots$  order along the  $t_2$  directions. A similar effect is found in the  $\frac{1}{4}$ -filled PEC state in the 2D anisotropic triangular lattice—there also  $V$  strengthens the  $\cdots 1100 \cdots$  CO provided  $V$  is not too large.<sup>16</sup> The most striking result of Fig. 5 is the very large spin gap that is obtained when both  $t_2/t_1$  and  $V$  are moderately large. We will return to this point later in Section 5.

## 4.2 Thermodynamics and spinon binding

To understand the thermodynamics of the zigzag ladder we present our results from complementary calculations of (i) wavenumber-dependent susceptibilities, and (ii) the nature of higher spin states. Finite-temperature calculations of susceptibilities here are done within the static undistorted lattice.

### 4.2.1 Temperature dependence of susceptibilities

We calculate wavenumber dependent charge ( $\chi_\rho(q)$ ), spin ( $\chi_\sigma(q)$ ), and bond susceptibilities ( $\chi_B(q)$ ), defined as

$$\chi_x(q) = \frac{1}{N} \sum_{j,k} e^{iq(j-k)} \int_0^\beta d\tau \langle O_j^x(\tau) O_k^x(0) \rangle. \quad (4)$$

In Eq. 4,  $O_j^\rho = n_{j,\uparrow} + n_{j,\downarrow}$ ,  $O_j^\sigma = n_{j,\uparrow} - n_{j,\downarrow}$ , and  $O_j^B = B_{j,j+1}$ , for charge, spin, and bond order susceptibilities, respectively.  $\beta$  is the inverse temperature in units of  $t_1$ . To facilitate comparison with 1D, the  $q$  is again taken to be one dimensional as in Eq. 2. The presence and periodicity of charge and bond order can be determined from divergences of the charge or bond-order susceptibility as  $\beta \rightarrow \infty$ . Within determinantal QMC methods finite  $V$  leads to a significantly worse Fermion sign problem and hence we present results only for nonzero  $U$  but  $V = 0$ . However, as shown in Fig. 5(a),  $V$  does not change the pattern of the bond distortion. We therefore expect that our results here are representative for arbitrary  $U$  and  $V$ .

Fig. 6 shows the bond, charge, and spin susceptibilities as a function of  $q$  and temperature for a  $N = 36$  site ladder with  $U = 4$ ,  $V = 0$ , and two representative values of  $t_2/t_1$ , 0.4 (Fig. 6(a)-(c)) and 1.4 (Fig. 6(d)-(f)). At low temperature, the bond, charge, and spin susceptibilities all peak at  $2k_F$ , consistent with period-four order of charges and bonds as expected. The  $2k_F$  peak in the spin susceptibility corresponds to the short-range AFM spin order found in the 1D  $\frac{1}{4}$ -filled chain. As seen in Fig. 6(c) and (f), the spin susceptibility converges to a finite value as  $q \rightarrow 0$  at low temperatures. This is consistent with the expectation that no SG exists in the ladder in the limit of zero e-p coupling. Several differences can be noted when comparing results for small and large  $t_2/t_1$ . First, the  $2k_F$  bond and charge response as  $T \rightarrow 0$  is stronger for small  $t_2/t_1$ . This reflects the larger amplitude distortion ( $\Delta n$  and bond order)

found in the 1D weakly-correlated limit (see Fig. 4(b)-(c)). The  $2k_F$  spin response becomes weaker with increasing  $t_2/t_1$ , and  $\chi_\sigma(q)$  is reduced for small  $q$ . These changes reflect the increasing strength of the spin-singlet bond along the  $t_1$  direction with increasing  $t_2/t_1$ , which in turn leads to the increase in  $\Delta_{ST}$ . For larger  $t_2/t_1$ , a broad plateau appears at  $q \approx 3\pi/4$  in the charge and spin susceptibilities. This plateau is however non-divergent—while it is significant at high and intermediate  $T$ , at low temperatures the  $2k_F$  response becomes stronger. We will show below that this plateau reflects the binding of spinon excitations.

Summarizing, the above numerical results show that in the zigzag ladder, no separate high-temperature ordering is expected; instead the ladder is metallic at high temperature and as temperature decreases a single transition to the PEC state with SG takes place. This is in contrast to what happens in 1D.<sup>22</sup>

### 4.2.2 Spinon excitations

The structure of excitations out of the ground state provides an alternate way to understand the thermodynamics of a strongly-correlated system. In the 1D limit, flipping one spin in the PEC results in two spinons which are unbound and hence separated by a distance of  $N/2$  sites on the lattice. We have performed self-consistent calculations within Eq. 1 of excited spin triplet ( $S = 1$ ) excitations to detect and study such spinon excitations in the zigzag ladder. Our calculations are for moderately large e-p interactions so that the widths of the charge-spin solitons are relatively narrow. This is necessary in order to prevent overlaps between the solitons. In Fig. 7 we show the charge and spin densities in the  $S = 1$  state of a 36 site zigzag ladder for small and large  $t_2/t_1$ . Spinon excitations are identified as defects in the  $\cdots 1100 \cdots$  charge order, and also from their large local spin densities.<sup>22</sup>

For small  $t_2/t_1$  (Fig. 7(a)), flipping a single spin results in two separated spinons as in the 1D chain. The repulsive interaction between spinons results in their separating to opposite positions on the periodic lattice. As indicated in the figure, each spinon occupies two lattice sites, and there occur both charge and spin modulations. The charge density at each spinon site is 0.5; the spin densities are also equal on the two sites. The PEC charge and bond distortions on either side of a spinon are out of phase with each other by two lattice sites. The charge densities on the two sites at the center of the are 0.5, 0.5 (see Fig. 7(a)). With increasing  $t_2/t_1$ , the lattice separation between the spinons decreases, indicating binding. For the e-p coupling of Fig. 7, at approximately  $t_2/t_1 \approx 1.0$  the bound spinons form a single excitation that occupies 4 lattice sites with approximately uniform charge density of 0.5 on each site (Fig. 7(b)). For spin states higher than 1 (not shown here), we found that spinons are bound in pairs; for example in the  $S = 2$  state there are two of the defects shown in Fig. 7(b), separated by the maximum possible lattice spacing. Spinon binding is usually associated with an increase in the singlet-triplet gap, and can thus explain the observation the (Fig. 4(d)) that for fixed  $V$ ,  $\Delta_{ST}$  increases with increasing  $t_2/t_1$ , even though  $\Delta n$  decreases at the same time.

The thermodynamic behavior is understood only when the complementary calculations of Fig. 6 and 7 are taken together. Fig. 7 shows spinon creation upon a single spin excitation, while the bond and charge susceptibilities show

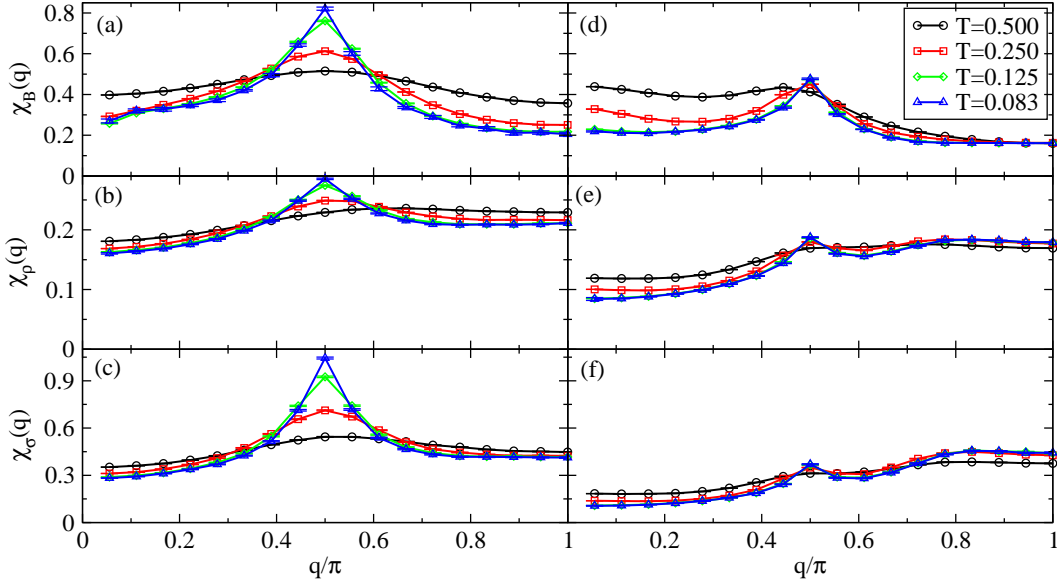


**Fig. 6.** (color online) Representative temperature-dependent QMC results for bond ((a) and (d)), charge ((b) and (e)), and spin susceptibilities ((c) and (f)) for a 36 site zigzag ladder with  $U = 4$ ,  $V = 0$ , and  $\alpha = 0$ .  $t_2/t_1$  is 0.4 in panels (a)-(c), and 1.4 in panels (d)-(f).

and high temperatures are dominated by high-spin configurations containing multiple spinons. Thus the signatures of spinons, including spinon binding can also be found in the finite-temperature QMC results of Fig. 6. In the 1D limit spinons have local  $4k_F$  charge or bond order.<sup>22</sup> As in the 1D chain (reference<sup>22</sup>), when  $t_2/t_1$  is small we find that the  $4k_F$  bond and charge susceptibilities *increase* with temperature (see Fig. 6(a)-(b) at  $q = \pi$ ).

When  $t_2/t_1$  is of order unity, several differences as seen in the susceptibilities that can be correlated with the binding of spinons shown in Fig. 7. First, at intermediate temperatures, the charge and spin susceptibilities have a broad plateau at  $q \approx 3\pi/4$ . When spinons bind, the larger size of these defects moves the charge and spin response away from  $4k_F$  and towards a smaller wavenumber. Second, in this parameter region the  $4k_F$  bond susceptibility remains small regardless of temperature and instead at higher temperatures a broad response from  $0 < q < \pi/2$  appears (Fig. 6(d)). This small- $q$  (long wavelength) bond order response is a result of increasing numbers of bound spinons created in high-spin configurations. Each high-spin configuration has multiple bound spinons equally separated from each other, giving a long-wavelength bond order distortion with  $0 < q < \pi/2$ . Related to this is the observation that  $\chi_B(2k_F)$  varies only weakly with temperature in the ladder limit. In the 1D limit, each spinon separates regions where the PEC is out of phase by two lattice units (Fig. 7(a)); due to this phase difference the introduction of spinons will lead to a rapid decrease in the  $2k_F$  response. On the other hand in the ladder limit, the PEC remains “in phase” on either side of bound spinons (Fig. 7(b)), resulting in a weaker temperature dependence of the  $2k_F$  bond susceptibility—bound spinons suppress the BCDW locally, but do not disturb the overall phase of the density wave as do single spinons.

### 5. Discussion

We have shown that the  $\frac{1}{4}$ -filled correlated zigzag ladder has the following properties: First, due to the geometry of

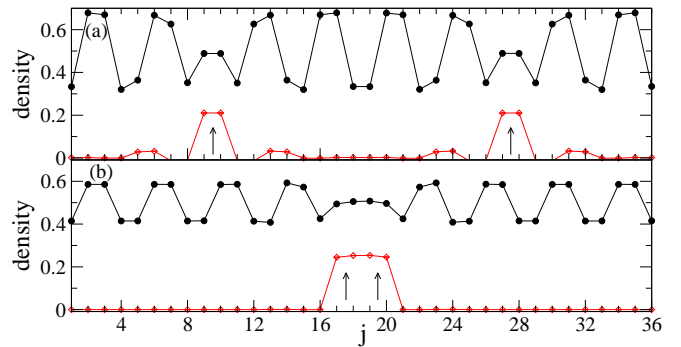


**Fig. 7.** (color online) MPS-QMC charge and spin density in the triplet state versus site index  $j$  along the  $t_1$  direction. Parameters are  $N = 36$ ,  $U = 6$ ,  $V = 1$ , and  $\alpha = 1.6$ . In panels (a) and (b),  $t_2/t_1 = 0.2$  and 1.4, respectively. Circles (diamonds) are charge (spin) density. Arrows indicate location of spinon defects (see text). Statistical errors are smaller than symbol sizes.

this lattice, the WC state driven by strong nearest-neighbor Coulomb interactions in 1D is strongly suppressed. Instead, a single PEC state with CO pattern  $\cdots 1100 \cdots$  occurs over a wide range of  $t_2/t_1$  ( $0 \leq t_2/t_1 \leq 1.707$ ). Second, unlike in the 1D  $\frac{1}{4}$ -filled band the bond order pattern in the zigzag ladder is  $SWMW$  for all Coulomb interactions, and the bond distortion  $SWSW'$  never occurs. Third, with increasing  $t_2/t_1$  from the 1D limit, the CO amplitude decreases for fixed  $V$  until it vanishes above a critical value. Surprisingly, the singlet-triplet gap increases in magnitude at the same time. We have shown that this increase is accompanied by the binding of spinon excitations. The singlet-triplet gap can be very large when  $t_2/t_1$  and  $V$  are both moderately large (see Fig. 5(d)). Finally, our QMC calculations show that in the zigzag ladder there is no distinct intermediate state between the low temperature PEC and the high temperature metallic state, and there is a single metal-insulator transition that is accompanied by simultaneous bond and charge distortions and spin gap. The existence of simultaneous transitions is expected here as the spin-singlet here is of the “intra-dimer” type as shown in Fig 2(c)-(d)



In the isotropic  $\frac{1}{4}$ -filled band 2D square lattice, adding a frustrating diagonal  $t'$  bond results in a transition from a uniform state to a paired PEC state once  $t'$  exceeds a critical value.<sup>15,16</sup> As with spin systems, the zigzag ladder provides a simple model for the study of the frustration-driven PEC state in 2D, with the difference that the frustration does not create the SG state in the ladder, but rather enhances the SG that is already present in the unfrustrated model. This enhancement can be large due to the cooperative interaction between the two kinds of electron-phonon interactions that are possible in the ladder, as shown in Fig. 3. We discuss below the implications of our work for understanding experiments on  $\frac{1}{4}$ -filled materials in general (including both 2D and 3D). We first consider specifically those materials which have been suggested to be ladders based on their crystal structures. We then also consider the broader class of  $\frac{1}{4}$ -filled band materials. Ideally, this second class of materials require understanding of the excitations and thermodynamics of the higher dimensional PEC, which is a much more formidable task than the ladder calculations. We nevertheless point out that broad conclusions can be drawn for these systems based on our current work. The majority of the materials we consider belong to the large family of low dimensional organic charge transfer solids (CTS), within which many examples of SG ground states are found with quasi-1D and 2D lattice.<sup>31</sup> We also point out a few inorganic  $\frac{1}{4}$ -filled materials that exhibit similar transitions.

### 5.1 $\frac{1}{4}$ -filled ladder candidates

While most ladder materials found have been  $\frac{1}{2}$ -filled,<sup>32</sup> the family of CTS materials  $(\text{DTTTF})_2\text{M}(\text{mnt})_2$ , where M is a metal ion, are likely candidates for  $\frac{1}{4}$ -filled band ladders.<sup>33</sup> In this series of compounds, the M=Au and M=Cu (for both the metal ion is diamagnetic) have been studied in most detail.<sup>33-37</sup> Structurally, these materials consist of pairs of DTTTF stacks, each with  $\frac{1}{4}$ -filled band of holes, separated by stacks of  $\text{M}(\text{mnt})_2$  which are Mott-Hubbard semiconductors with  $\frac{1}{2}$ -filled electron bands. It is then likely that the each pair of DTTTF stacks behaves as ladders. Note that the stack direction corresponds to the  $t_2$  direction within our model, and hence these systems lie in the parameter regime  $t_2 > t_1$ . The very large<sup>36</sup>  $T_{\text{SG}}$  in  $(\text{DTTTF})_2\text{Au}(\text{mnt})_2$  ( $\sim 70$  K) and  $(\text{DTTTF})_2\text{Cu}(\text{mnt})_2$  ( $\sim 90$  K), which are nearly an order of magnitude larger than the spin-Peierls transition temperatures in the 1D  $\frac{1}{4}$ -filled systems,<sup>38</sup> supports the conjecture that these systems are ladders.

The MI and SG transitions are, however, distinct in these compounds, which would argue against the zigzag ladder picture, at least its simplest version. For M=Au, a broad MI transition occurs at  $T_{\text{MI}} \approx 220$  K, followed by a decrease in the magnetic susceptibility at 70 K.<sup>34</sup> Below the MI transition, diffuse X-ray scattering at  $b^*/2$  indicates dimerization along  $t_2$ , but broad line widths suggest the dimerization order is not long-ranged.<sup>34</sup> The M=Cu salt is isostructural to the Au salt with slightly smaller lattice parameters due to the smaller metal ion. The MI transition for M=Cu occurs at 235 K, and unlike the Au salt is a sharp, second-order phase transition that is accompanied by doubling of the unit cell in the ladder direction.<sup>36</sup> Changes in the optical properties at  $T_{\text{MI}}$  and  $T_{\text{SG}}$  for the two salts are also different.<sup>35,37</sup> For M=Au, at  $T_{\text{MI}}$  symmetry breaking occurs along the rung direction (perpen-

dicular to the DTTTF stacks), while at  $T_{\text{SG}}$ , symmetry breaking is predominantly along the stacks.<sup>35</sup> In contrast, optical response indicates symmetry breaking in both rung and stack directions at  $T_{\text{MI}}$  for M=Cu.<sup>37</sup>

We believe that the  $\frac{1}{4}$ -filled band zigzag ladder model is nevertheless a valid description for both M = Au and Cu at low temperatures. The only other competing model for these systems is the rectangular ladder model,<sup>35</sup> wherein each DTTTF molecule is coupled to a single other such molecule on the neighboring stack. Such a description would be against the known crystal structures.<sup>33</sup> Furthermore, within the rectangular ladder model, there needs to occur a high temperature metal-insulator transition accompanied by in-phase bond dimerization, such that each dimer of DTTTF molecules has a single electron; the ladder after dimerization would be akin to rectangular spin ladder, which has SG for all interstack spin exchange. The two stacks need to be identical within the model and hence there is no symmetry breaking within the rectangular ladder scenario along the rung direction at any temperature. Neither is there any CO within the model, in contradiction to what is found in optical measurements.<sup>37</sup>

There can be several different reasons why the high temperature MI transition occurs within the zigzag ladder scenario. First, muon spin rotation experiments suggest significant interladder coupling,<sup>39</sup> that has been ignored in our isolated ladder model. Second, our model does not take into account the temperature-dependent lattice expansion that is common to CTS crystals. Note that lattice expansion will affect the interstack hopping  $t_1$  much more strongly than the intrastack hopping  $t_2$ . It is then conceivable that at high temperatures the interstack distance is large enough (and  $t_1$  is small enough) that  $t_2/t_1$  is greater than the critical value 1.707 and the systems behave as independent chains. The lattice contracts at reduced temperatures, increasing  $t_1$  and reducing  $t_2/t_1$ , when the systems exhibit zigzag ladder behavior. This would require  $t_2/t_1$  close to 1.7 in the experimental systems, which is indeed close to ratio of the calculated hopping integrals for the M = Au system.<sup>34</sup> As seen in Fig. 4(d), large  $t_2/t_1$  would be in agreement with the unusually large SG seen in the  $(\text{DTTTF})_2\text{M}(\text{mnt})_2$ . There are however additional complications. During the synthesis of the  $(\text{DTTTF})_2\text{M}(\text{mnt})_2$  salt, the 1:1 salt  $(\text{DTTTF})\text{M}(\text{mnt})_2$  is also produced and crystals of the 1:2 salt must therefore be separated from this mixture for experiments.<sup>36</sup> Relative to other CTS, available experimental data is thus more limited. Experimental determinations of the pattern of the CO below  $T_{\text{SG}}$  (and above, if any), and of the temperature-dependent lattice distortion are necessary for resolution of the above issues.

### 5.2 General classification of $\frac{1}{4}$ -filled materials

As discussed in Section 3.1, in 1D the SG and MI transitions are distinct when the ground state broken-symmetry state has the bond pattern SWSW', but are coupled together in a single transition when the bond pattern is SMWM as occurs in the zigzag ladder we have considered here. In 1D, the strength of e-e interactions determines which bond pattern is favored. As SG transitions are found in a number of  $\frac{1}{4}$ -filled materials with 2D as well as 3D lattices, generalizations of these results to higher lattice dimensionality are of great interest. Our results in Section 4 for the zigzag lad-

Material	D-n	T <sub>SG</sub> (K)	T <sub>CB</sub> (K)	Ref.
MEM(TCNQ) <sub>2</sub>	1D-2	17	335	42,43
(TMTTF) <sub>2</sub> PF <sub>6</sub>	1D-2	19	70	38,44
$\theta$ -(ET) <sub>2</sub> RbZn(SCN) <sub>4</sub>	2D-2	20	195	45-48
EtMe <sub>3</sub> P[Pd(dmit) <sub>2</sub> ] <sub>2</sub>	2D-2	25	> 300	49,50
$\beta'$ -DODHT) <sub>2</sub> PF <sub>6</sub>	2D-2	40	255	51,52
(DMe-DCNQI) <sub>2</sub> Ag	1D-2	80	100	53
$\alpha$ -NaV <sub>2</sub> O <sub>5</sub>	2D-1	34	34	54
$\alpha'$ -(ET) <sub>2</sub> I <sub>3</sub>	2D-1	135	135	55,56
(BDTFP) <sub>2</sub> PF <sub>6</sub> (PhCl) <sub>0.5</sub>	1D-1	175	175	57-59
CuIr <sub>2</sub> S <sub>4</sub>	3D-1	230	230	60,61
(EDO-TTF) <sub>2</sub> PF <sub>6</sub>	1D-1	280	280	62,63

**Table I.**  $\frac{1}{4}$ -filled materials with spin gapped ground states. For each the dimensionality and number of transitions D-n, spin-gap transition temperature T<sub>SG</sub>, charge-bond ordering temperature T<sub>CB</sub>, and references are listed.

strength does *not necessarily* determine the bond distortion pattern and thermodynamics—lattice structure and frustration are also important.

We point out an empirical criterion here that rationalizes separate versus coupled SG–MI transitions in  $\frac{1}{4}$ -filled band materials at large, that we arrive at by simply extrapolating from the 1D and zigzag ladder results. Our observation is that if the low temperature structure is such that the singlet bond is interdimer, and the strongest bond is between intradimer charge-rich and charge-poor sites (Fig. 2(b)), there occur distinct transitions involving charge and spin degrees of freedom. Conversely, if the intradimer bond is between a pair of charge-rich sites (Fig. 2(c)), and the SG is due to intradimer spin-singlets, there is a single coupled SG–MI transition. In this latter case in general T<sub>SG</sub> is high. The first of these two observations was noted previously by Mori.<sup>40</sup> We do not have any microscopic calculation to justify these conclusions for 2D and 3D; they are based on the mappings of Fig. 2. In Table I we give a list of materials for which the bond and/or charge ordering pattern below T<sub>SG</sub> is known. In all cases our simple criterion appears to be valid (see below). Two of the entries require additional explanation. (TMTTF)<sub>2</sub>PF<sub>6</sub> is already insulating at room temperature because of lattice dimerization; the high temperature CO at 70 K here is of the WC type, but there is strong redistribution of the charge below T<sub>SG</sub>,<sup>41</sup> clearly placing this system into the category of materials that undergoes two transitions.<sup>22</sup> The low T<sub>SG</sub> is also a signature of this. The situation with  $\alpha'$ -NaV<sub>2</sub>O<sub>5</sub> is exactly the opposite. This system is also insulating already at high temperature, but now the charge-ordering and spin-gap transitions occur at the same temperature, indicating that these transitions are coupled. While Table I is meant to be representative and not comprehensive, we are unaware of examples where our criterion fails. We describe individual materials in detail below.

### 5.2.1 Two transitions: inter-dimer singlet formation

We have previously discussed quasi-1D CTS where two transitions occur.<sup>22</sup> MEM(TCNQ)<sub>2</sub> is one example where the low temperature bond pattern has been well characterized by neutron scattering.<sup>43</sup> In MEM(TCNQ)<sub>2</sub>, the MI transition occurs near room temperature at T<sub>MI</sub>=335 K, followed by a SG transition at T<sub>SG</sub>=17.4 K.<sup>42,43</sup> The bond pattern at low temper-

ature is SWSW'.<sup>43</sup> The (TMTTF)<sub>2</sub>X series is another quasi-1D example where CO and SG occur at different temperatures.<sup>22,44,64–66</sup>

In the 2D  $\theta$ -(BEDT-TTF)<sub>2</sub>MM'(SCN)<sub>4</sub> series, CO occurs at the high temperature MI transition<sup>45,46</sup> followed by the SG transition at T<sub>SG</sub> ~20 K.<sup>45,47,48</sup> X-ray studies in the temperature range T<sub>SG</sub> < T < T<sub>CO</sub> show that the strongest bond orders in the 2D BEDT-TTF layers are between molecules with large and small charge density (see Fig. 7 in reference<sup>47</sup>). These and lower temperature X-ray results<sup>48</sup> have indicated that the spin-singlets in the SG phase are located on the inter-dimer bonds, as in the SWSW' bond pattern in 1D.

Yet another 2D material that very clearly shows two transitions and in which the charge-bond distortion patterns are known is EtMe<sub>3</sub>P[Pd(dmit)<sub>2</sub>]<sub>2</sub>.<sup>49,50</sup> The material is semiconducting already at 300 K (T<sub>MI</sub> > 300 K). The magnetic susceptibility at high temperatures corresponds to that of a Heisenberg antiferromagnet on a triangular lattice with J = 250 K. Below a relatively low T<sub>SG</sub>=25 K the system enters a distorted phase, with the intermolecular bond distortion pattern clearly of the dimerized dimer type, and the strongest bonds between charge-rich and charge-poor sites.<sup>50</sup> This material undergoes superconducting transition under pressure.<sup>67</sup>

### 5.2.2 Coupled transitions: intra-dimer singlet formation

In cases where T<sub>MI</sub> and T<sub>SG</sub> coincide, the spin gap transition temperature tends to be quite high. Examples here include (EDO-TTF)<sub>2</sub>X, which shows a first order MI transition at high temperature, 280 K for X=PF<sub>6</sub> and 268 K for X=AsF<sub>6</sub>.<sup>62</sup> This transition coincides with T<sub>SG</sub>.<sup>62</sup> Optical experiments determined that the charge order pattern in the low temperature phase is  $\cdots 1100 \cdots$ , with the strongest bond between molecules with large charge density.<sup>63</sup> A coupled SG–MI transition occurs at T<sub>MI</sub>=175 K in (BDTFP)<sub>2</sub>PF<sub>6</sub>(PhCl)<sub>0.5</sub>.<sup>57</sup> While structurally (BDTFP)<sub>2</sub>PF<sub>6</sub>(PhCl)<sub>0.5</sub> appears to be ladder-like,<sup>18,57</sup> X-ray<sup>58</sup> and optical measurements<sup>59</sup> show that in the low-temperature phase tetramerization takes place along the stacks with the SMWM bond pattern.<sup>58</sup> The coupled SG–MI transitions found in these two materials are consistent with our criterion above.

Beyond quasi-1D materials, in the 2D CTS examples can be found with coupled transitions, which also typically take place at a relatively high temperature. In  $\alpha$ -(BEDT-TTF)<sub>2</sub>I<sub>3</sub> T<sub>SG</sub>=135 K coinciding with the MI transition.<sup>55</sup> Similar to (EDO-TTF)<sub>2</sub>X, the SG–MI transition is first order and coincides with a large structural change.<sup>56</sup> In the low temperature phase, the strongest bond is again between the sites of largest charge density.<sup>56</sup>

Similar transitions are observed in inorganic  $\frac{1}{4}$ -filled materials as well. The inorganic spinel CuIr<sub>2</sub>S<sub>4</sub> is one example in which the Ir-ions form the active sites with  $\frac{3}{4}$ -filled electron band ( $\frac{1}{4}$ -filled hole band).<sup>61</sup> In CuIr<sub>2</sub>S<sub>4</sub> a coupled SG–MI transition occurs at 230 K, below which the criss-cross chains of Ir-ions are charge-ordered as Ir<sup>4+</sup>-Ir<sup>4+</sup>-Ir<sup>3+</sup>-Ir<sup>3+</sup>, with the strongest bonds between the spin  $\frac{1}{2}$  hole-rich Ir<sup>4+</sup> ions and weakest bonds between the spin 0 hole-poor Ir<sup>3+</sup> ions.<sup>60,61</sup> A more complex coupled transition occurs in  $\alpha'$ -NaV<sub>2</sub>O<sub>5</sub>, where a coupled CO-SG transition occurs at 34 K within an insulating phase. Structurally  $\alpha'$ -NaV<sub>2</sub>O<sub>5</sub> consists of rectangular V-



ion based ladders linked by zigzag V-V bonds. Below the transition the V-ions are charge disproportionated and there occurs a period-4  $V^{4+}-V^{4+}-V^{5+}-V^{5+}$  CO within the zigzag links between the rectangular ladders. Once again, the strongest bonds are between the spin  $\frac{1}{2}$  electron-rich  $V^{4+}$  ion pairs and the weakest bonds between the spin 0 electron-poor  $V^{5+}$  ion pairs,<sup>68,69</sup> in agreement with our criterion for coupled CO-SG transition.

### 5.3 Possible relationship with superconductivity

We have recently suggested that superconductivity in strongly-correlated  $\frac{1}{4}$ -filled systems is due to a transition from an insulating PEC state to a paired-electron liquid.<sup>15,16,70</sup> Within this model, the spin-singlets of the PEC become mobile with further increase in frustration. The fundamental theoretical picture is then analogous to bipolaron theories of superconductivity,<sup>71</sup> with two differences: (i) the pairing in our model is driven by antiferromagnetic correlations (as opposed to very strong e-p interactions that screen out the short-range Coulomb repulsion), and (ii) nearly all the carriers are involved in the pairing. The effective mass of the spin-bonded pairs is an important parameter, and overly strong binding will reduce pair mobility. This would suggest that superconductivity is *more likely* in materials with inter-dimer singlets. As noted in the above, such systems tend to have the dimerized dimer structure. In contrast, in those materials with intradimer singlets that form at high temperature, the stronger pair binding would lead to a pair mobility too low to achieve superconductivity—in these cases the ground state would remain an insulating spin-gapped PEC with charge and bond order. It is interesting to note that such a correlation was suggested from empirical observations alone by Mori.<sup>40</sup>

## 6. Acknowledgments

This work was supported by the US Department of Energy grant DE-FG02-06ER46315. RTC thanks A. Sandvik for helpful discussions regarding the MPS-QMC method. RTC thanks the University of Arizona, the Boston University Condensed Matter Theory Visitor's program, and the Institute for Solid State Physics of the University of Tokyo for hospitality while on sabbatical.

## Appendix A: MPS-QMC method

Matrix-product states are best known as the class of wavefunctions ultimately reached by the DMRG process<sup>72</sup> and provide highly efficient representations of wavefunctions for quasi-1D quantum systems. An alternate set of methods to DMRG has recently emerged which combines a MPS wavefunction representation with MC sampling.<sup>26,73</sup> In this approach, rather than the renormalization procedure used by DMRG, Monte Carlo (MC) sampling is used to evaluate expectation values of the MPS wavefunction. The use of MC has certain advantages, such as potentially better computational scaling,<sup>26</sup> and the ease with which the method can be parallelized through trivial parallelization of the MC averaging.

The MPS-QMC method we use is described in Reference,<sup>26</sup> where it was applied to the 1D quantum Ising model in a transverse field. Here we show that the method can successfully be applied to more complicated Fermion Hamiltonians. In the MPS-QMC method, the ground state energy is estimated by

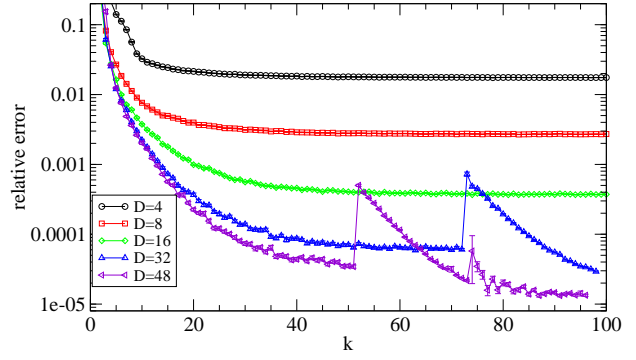


**Fig. A-1.** (color online) Relative error in the ground state energy using MPS-QMC as a function of number of QMC steps  $k$  and matrix size  $D$  for a 20 site ladder with periodic boundary conditions and  $t_1 = t_2 = 1$ ,  $U = 6$ ,  $V = 1$ , and  $\alpha = 0$ . Calculations for  $D=4, 8$ , and  $16$  were single optimization runs, while those for  $32$  and  $48$  were restarted after  $50\text{--}75$  steps (see text).

system is written as

$$|\Psi\rangle = \sum_{\{S\}} \text{Tr}[A_1(s_1)A_2(s_2)\cdots A_N(s_N)]|s_1s_2\cdots s_N\rangle. \quad (\text{A}\cdot 1)$$

In Eq. A-1,  $|S\rangle = |s_1s_2\cdots s_N\rangle$  is a single many-electron configuration where the state on each site  $i$  is  $s_i$ . In the spin- $\frac{1}{2}$  model considered in Reference<sup>26</sup>  $s_i = \pm 1$ . For the Hubbard model  $s_i$  takes four possible values corresponding to either empty, spin-up, spin-down, or doubly occupied states.  $A_j$  are  $D \times D$  matrices, where  $D$  is an adjustable parameter. As we study ground state configurations containing spinon defect states that break translational symmetry, we keep separate matrices  $A_i(s_i)$  for each lattice site. In the MPS-QMC method the matrix elements of the matrices  $A_i(s_i)$  are stochastically optimized to minimize the expectation value of  $H$ .

The method may be summarized as follows: the matrix elements  $a_{ij}^k(s_k)$  are first initialized to hold random values. Matrices are normalized so that their Frobenius norm is unity,  $\sqrt{\text{Tr}(AA^T)} = 1$ . The expectation values of the energy and derivatives of the energy with respect to  $a_{ij}^k(s_k)$ ,  $k = 1 \cdots N$ , are evaluated using MC sampling and a Metropolis acceptance probability. Configurations are sampled according to the weight  $W^2(S)$  with

$$W(S) = \text{Tr}[A_1(s_1)A_2(s_2)\cdots A_N(s_N)]. \quad (\text{A}\cdot 2)$$

The MC updates used to sample the configurations  $\{S\}$  interchange electrons between neighboring sites, i.e.  $\{ \uparrow \downarrow \} \rightleftharpoons \{ \downarrow \uparrow \}$ . In such a process, two matrices in Eq. A-2 are changed. The changed weight,  $W(S')$ , may be efficiently generated by saving a series of “right” and “left” matrix products, and sequentially attempting updates<sup>26</sup> for sites  $i = 1 \cdots N$ . The estimates of the derivatives are used to optimize the initial random matrices using a stochastic optimization scheme.<sup>26</sup> The calculation is divided into a series of steps  $k = 0, 1, 2, \dots$ . At each step, the amplitude of the stochastic noise is decreased, and the number of MC samples is increased to provide increasingly accurate derivatives as the minimum energy is approached. The overall operation count of the MPS-QMC method scales more favorably with the matrix size ( $\propto D^3$ ) for periodic systems than does traditional DMRG.<sup>26</sup>

Fig. A-1 and Table A-1 compare the accuracy of MPS-QMC against exact diagonalization for the energy, kinetic en-

$D$	E	KE	PE	$S_\sigma(\pi/2)$
4	-0.92942(1)	-1.46896(4)	0.53954(4)	0.15115(3)
8	0.940809(7)	-1.46732(4)	0.52651(4)	0.15280(3)
16	-0.942555(2)	-1.46824(4)	0.52568(4)	0.15608(2)
32	-0.9426859(6)	-1.46818(3)	0.52549(3)	0.15647(4)
48	-0.9427005(5)	-1.46821(3)	0.52551(3)	0.15649(4)
ED	-0.9427135	-1.468223	0.525510	0.156520

**Table A-1.** Comparison of the ground state energy per site, kinetic energy per site, potential energy per site, and spin structure factor  $S_\sigma(\pi/2)$  between MPS-QMC and exact diagonalization a 20 site ladder with periodic boundary conditions and  $t_2/t_1 = 1$ ,  $U = 6$ , and  $V = 1$ . Statistical Monte Carlo sampling errors in the last digit are shown in parenthesis.

energy, potential energy, and spin structure factor, defined as

$$S_\sigma(q) = \frac{1}{N} \sum_{jl} e^{iq(j-l)} \langle (n_{j\uparrow} - n_{j\downarrow})(n_{l\uparrow} - n_{l\downarrow}) \rangle. \quad (\text{A} \cdot 3)$$

Fig. A-1 shows the relative error in the ground state energy as a function of the number of sampling blocks for a 20-site ladder with  $t_1 = t_2 = 1$ ,  $U = 6$  and  $V = 1$ . Each step  $k$  of the algorithm is further divided into a number  $n$  of blocks consisting of  $m$  Monte Carlo updates each, with the matrices  $A_i(S_i)$  updated using the calculated derivatives after each block.  $n$  and  $m$  are increased as  $n = kn_0$  and  $m = km_0$ , with  $n_0 = 25$  and  $m_0 = 100$  in Fig. A-1. We find that larger matrix sizes are needed here compared to those typically used for spin models; this is expected because of the greater number of quantum states per site. However, even with the much larger number of parameters (matrices are also site-dependent in our calculations) the stochastic optimization method performs well. Comparing with  $N = 20$  site exact results, relative energy accuracy of order  $10^{-5}$  is achievable with  $D = 48$ . As shown in Table A-1, local quantities such as the kinetic energy (bond order) and potential energy converge quite rapidly with  $D$ . As expected, long-range correlations require larger  $D$  for similar numerical accuracy. The 36-site calculations presented in Section 4 used  $D = 48$  matrices.

In order to treat the e-p terms in Eq. 1, we use the an iterative self-consistent method<sup>21</sup> to update the bond distortions  $\Delta_{i,j}$ . The self-consistency equations for the lattice are updated once every MC block following the calculation of charge densities and bond orders. Self-consistent MPS-QMC results were verified against exact self-consistent calculations.

## Appendix B: Finite-size scaling

For the results reported in Figs. 4 and 5 we performed finite-size scaling from calculations on 20, 28, 36, and 60 site ladders. The 20 site data was from exact lanczos calculations and larger system data from the MPS-QMC method detailed in Appendix A using a matrix size of  $D = 48$ . Here we give further details of our extrapolation procedure.

Because the properties of quasi-1D systems display an alternation with  $N$  as the chain length increases, we have chosen only ladders with  $4n + 2$  electrons. These systems also have closed shells in the noninteracting limit. The PEC ground state further requires that  $N$  be a multiple of four. Fig. B-1(a) shows the finite-size extrapolation for the charge disproportionation  $\Delta n$  for both small and large  $t_2/t_1$ .  $\Delta n$  as well as  $r_4$  and  $E_s$  (not shown here) change only by a small amount from 20 to 60 sites. Fig. B-1(b) shows the finite size scaling of the

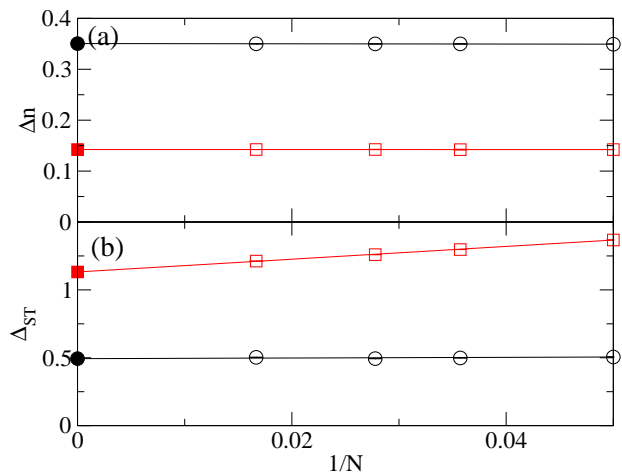


**Fig. B-1.** (color online) Finite-size scaling of observables for  $U = 6$ ,  $V = 1$ , and  $\alpha = 1.6$ . Circles (squares) are for  $t_2/t_1 = 0.2$  ( $t_2/t_1 = 1.6$ ).  $N$  is the number of lattice sites. Filled symbols show the extrapolated values of the observables. Panel (a) shows the charge disproportionation  $\Delta n$  and panel (b) the singlet-triplet gap  $\Delta_{ST}$ . Lines are least-squares fits to the points.

singlet-triplet gap  $\Delta_{ST}$ . Errors in the extrapolation of  $\Delta_{ST}$  are larger than those in  $\Delta n$ ,  $r_4$ , and  $E_s$ , because the gap is calculated from the energy difference of separate  $S = 0$  and  $S = 1$  calculations, each of which have different lattice configurations that are optimized self-consistently. This accounts for the larger error bars in Fig. 4(d) compared to Fig. 4(a)-(c).

- 1) *Frustrated Spin Systems*, ed. H. Diep (World Scientific, Singapore, 2004).
- 2) *Introduction to Frustrated Magnetism*, ed. C. Lacroix, P. Mendels, and F. Mila (Springer-Verlag, Berlin, 2011).
- 3) C. K. Majumdar and D. K. Ghosh: *J. Math. Phys.* **10** (1969) 1388.
- 4) C. K. Majumdar and D. K. Ghosh: *J. Math. Phys.* **10** (1969) 1399.
- 5) K. Okamoto and K. Nomura: *Phys. Lett. A* **169** (1992) 433.
- 6) R. Chitra, S. pati, H. R. Krishnamurthy, D. Sen, and S. Ramasesha: *Phys. Rev. B* **52** (1995) 6581.
- 7) B. S. Shastry and B. Sutherland: *Phys. Rev. Lett.* **47** (1981) 964.
- 8) E. Sorensen, I. Affleck, D. Augier, and D. Poilblanc: *Phys. Rev. B* **58** (1998) R14701.
- 9) S. R. White and I. Affleck: *Phys. Rev. B* **54** (1996) 9862.
- 10) C. Itoi and S. Qin: *Phys. Rev. B* **63** (2001) 224423.
- 11) M. Kumar, Z. G. Soos, D. Sen, and S. Ramasesha: *Phys. Rev. B* **81** (2010) 104406.
- 12) H. Kino and H. Fukuyama: *J. Phys. Soc. Jpn.* **64** (1995) 2726.
- 13) K. Kanoda: *J. Phys. Soc. Jpn.* **75** (2006) 051007.
- 14) B. J. Powell and R. H. McKenzie: *Rep. Progr. Phys.* **74** (2011) 056501.
- 15) H. Li, R. T. Clay, and S. Mazumdar: *J. Phys.: Condens. Matter* **22** (2010) 272201.
- 16) S. Dayal, R. T. Clay, H. Li, and S. Mazumdar: *Phys. Rev. B* **83** (2011) 245106.
- 17) J. Merino, H. Seo, and M. Ogata: *Phys. Rev. B* **71** (2005) 125111.
- 18) R. T. Clay and S. Mazumdar: *Phys. Rev. Lett.* **94** (2005) 207206.
- 19) K. C. Ung, S. Mazumdar, and D. Toussaint: *Phys. Rev. Lett.* **73** (1994) 2603.
- 20) M. Kuwabara, H. Seo, and M. Ogata: *J. Phys. Soc. Jpn.* **72** (2003) 225.
- 21) R. T. Clay, S. Mazumdar, and D. K. Campbell: *Phys. Rev. B* **67** (2003) 115121.
- 22) R. T. Clay, R. P. Hardikar, and S. Mazumdar: *Phys. Rev. B* **76** (2007) 205118.
- 23) K. Yoshimi, H. Seo, S. Ishibashi, and S. E. Brown: *Phys. Rev. Lett* **108** (2012) 096402.
- 24) S. Mazumdar, R. T. Clay, and D. K. Campbell: *Phys. Rev. B* **62** (2000) 13400.

- 25) Y. Otsuka, H. Seo, Y. Motome, and T. Kato: J. Phys. Soc. Jpn. **77** (2008) 113705.
- 26) A. Sandvik and G. Vidal: Phys. Rev. Lett. **99** (2007) 220602.
- 27) S. R. White: Phys. Rev. Lett. **69** (1992) 2863.
- 28) S. R. White: Phys. Rev. B **48** (1993) 10345.
- 29) J. E. Hirsch and D. J. Scalapino: Phys. Rev. B **29** (1984) 5554.
- 30) E. Y. Loh Jr. and J. E. Gubernatis: Stable numerical simulations of models of interacting electrons in condensed-matter physics. In W. Hanke and Y. V. Kopaev (eds), *Electronic Phase transitions*, pp. 177–235. Elsevier, 1992.
- 31) T. Ishiguro, K. Yamaji, and G. Saito: *Organic Superconductors* (Springer-Verlag, New York, 1998).
- 32) E. Dagotto and T. M. Rice: Science **271** (1996) 618.
- 33) C. Rovira: Chem. Eur. J. **6** (2000) 1723.
- 34) E. Ribera, C. Rovira, J. Veciana, J. Tarreés, E. Canadell, R. Rousseau, E. Molins, M. Mas, J. P. Schoeffel, J. P. Pouget, J. Morgado, R. T. Henriques, and M. Almeida: Chem. Eur. J **5** (1999) 2025.
- 35) R. Wesolowski, J. T. Haraldsen, J. L. Musfeldt, T. Barnes, M. Mas-Torrent, C. Rovira, R. T. Henriques, and M. Almeida: Phys. Rev. B **68** (2003) 134405.
- 36) X. Ribas, M. Mas-Torrent, A. Prez-Bentez, J. C. Dias, H. Alves, E. B. Lopes, R. T. Henriques, E. Molins, I. C. Santos, K. Wurst, P. Foury-Leylekian, M. Almeida, J. Veciana, and C. Rovira: Adv. Functional Materials **15** (2005) 1023.
- 37) J. L. Musfeldt, S. Brown, S. Mazumdar, R. Clay, M. Mas-Torrent, C. Rovira, J. C. Dias, R. T. Henriques, and M. Almeida: Solid State Sciences **10** (2008) 1740.
- 38) J. P. Pouget: Semiconductors and Semimetals **27** (1988) 87.
- 39) D. Arçon, A. Lappas, S. Margadonna, K. Prassides, E. Ribera, J. Veciana, C. Rovira, R. T. Henriques, and M. Almeida: Phys. Rev. B **60** (1999) 4191.
- 40) T. Mori: Bull. Chem. Soc. Jpn. **72** (1999) 2011.
- 41) T. Nakamura, K. Furukawa, and T. Hara: J. Phys. Soc. Jpn. **76** (2007) 064715.
- 42) S. Huizinga, J. Kommandeur, G. A. Sawatzky, B. T. Thole, K. Kopinga, W. J. M. de Jonge, and J. Roos: Phys. Rev. B **19** (1979) 4723.
- 43) R. J. J. Visser, S. Oostra, C. Vettier, and J. Voiron: Phys. Rev. B **28** (1983) 2074.
- 44) F. Nad and P. Monceau: J. Phys. Soc. Jpn. **75** (2006) 051005. and references therein.
- 45) H. Mori, S. Tanaka, and T. Mori: Phys. Rev. B **57** (1998) 12023.
- 46) K. Miyagawa, A. Kawamoto, and K. Kanoda: Phys. Rev. B **62** (2000) R7679.
- 47) M. Watanabe, Y. Noda, Y. Nogami, and H. Mori: J. Phys. Soc. Jpn. **73** (2004) 116.
- 48) M. Watanabe, Y. Noda, Y. Nogami, and H. Mori: J. Phys. Soc. Jpn. **76** (2007) 124602.
- 49) R. Kato: J. Am. Chem. Soc. **128** (2006) 10016.
- 50) M. Tamura, A. Nakao, and R. Kato: J. Phys. Soc. Jpn. **75** (2006) 093701.
- 51) H. Nishikawa, T. Morimoto, T. Kodama, I. Ikemoto, K. Kikuchi, J. Yamada, H. Yoshino, and K. Murata: J. Am. Chem. Soc. **124** (2002) 730.
- 52) H. Nishikawa, Y. Sato, K. Kikuchi, T. Kodama, I. Ikemoto, J. Yamada, H. Oshio, R. Kondo, and S. Kagoshima: Phys. Rev. B **72** (2005) 052510.
- 53) H.-P. Werner, J. U. von Schütz, H. C. Wolf, R. Kremer, M. Gehrke, A. Aumüller, P. Erk, and S. Hünig: Solid St. Comm. **65** (1988) 809.
- 54) M. Isobe and Y. Ueda: J. Phys. Soc. Jpn. **65** (1996) 1178.
- 55) B. Rothaemel, L. Forró, J. Cooper, J. Schilling, M. Weger, P. Bele, H. Brunner, D. Schweitzer, and H. Keller: Phys. Rev. B **34** (1986) 704.
- 56) T. Kakiuchi, Y. Wakabayashi, H. Sawa, T. Takahashi, and T. Nakamura: J. Phys. Soc. Jpn. **76** (2007) 113702.
- 57) T. Ise, T. Mori, and K. Takahashi: J. Mater. Chem. **11** (2001) 264.
- 58) M. Uruichi, K. Yakushi, T. Shirahata, K. Takahashi, T. Mori, and T. Nakamura: J. Mater. Chem. **12** (2002) 2696.
- 59) M. Uruichi, K. Yakushi, T. Shirahata, and K. Takahashi: Synth. Metals **133–134** (2003) 407.
- 60) P. G. Radaelli, Y. Horibe, M. J. Gutmann, H. Ishibashi, C. H. Chen, R. M. Ibberson, Y. Koyama, Y.-S. Hor, V. Kiryukhin, and S.-W. Cheong: Nature **416** (2002) 155.
- 61) D. I. Khomskii and T. Mizokawa: Phys. Rev. Lett. **94** (2005) 156402.
- 62) A. Ota, H. Yamochi, and G. Saito: J. Mater. Chem. **12** (2002) 2600.
- 63) O. Drozdova, K. Yakushi, K. Yamamoto, A. Ota, H. Hideki, Y. Yamochi, G. Saito, H. Tashiro, and D. B. Tanner: Phys. Rev. B **70** (2004) 075107.
- 64) D. S. Chow, F. Zamborszky, B. Alavi, D. J. Tantillo, A. Baur, C. A. Merlic, and S. E. Brown: Phys. Rev. Lett. **85** (2000) 1698.
- 65) P. Foury-Leylekian, D. L. Bolloc'h, B. Hennion, S. Ravy, A. Moradpour, and J.-P. Pouget: Phys. Rev. B **70** (2004) 180405. and references therein.
- 66) S. Fujiyama and T. Nakamura: J. Phys. Soc. Jpn. **75** (2006) 014705.
- 67) Y. Shimizu, H. Akimoto, H. Tsujii, A. Tajima, and R. Kato: Phys. Rev. Lett. **99** (2007) 256403.
- 68) M. V. Mostovoy and D. I. Khomskii: Solid St. Commun. **113** (2009) 159.
- 69) B. Edegger, H. G. Evertz, and R. M. Noack: Phys. Rev. Lett. **96** (2006) 146401.
- 70) S. Mazumdar and R. T. Clay: Phys. Rev. B **77** (2008) 180515(R).
- 71) A. S. Alexandrov and N. F. Mott: *High Temperature Superconductors And Other Superfluids* (Taylor and Francis, London, 1994).
- 72) S. Östlund and S. Rommer: Phys. Rev. Lett. **75** (1995) 3537.
- 73) N. Schuch, M. M. Wolf, F. Verstraete, and J. I. Cirac: Phys. Rev. Lett. **100** (2008) 040501.